Ceramics International 42 (2016) 8488–8494

Contents lists available at ScienceDirect

Ceramics International

journal homepage: www.elsevier.com/locate/ceramint

Microstructure effects on $BaTiO_3/BaTi_{0.8}Zr_{0.2}O_3$ composites properties

Thiago Martins Amaral [a,*], Eduardo Antonelli [c], Diego Alejandro Ochoa [b], José Eduardo García [b], Antonio Carlos Hernandes [a]

[a] Grupo de Crescimento de Cristais e Materiais Cerâmicos, Physics Institute of São Carlos, University of São Paulo, 13560-970 São Carlos, SP, Brazil
[b] Department of Physics, Universitat Politècnica de Catalunya – BarcelonaTech, 08034 Barcelona, Spain
[c] Science and Technology Institute, Federal University of São Paulo – UNIFESP, São José dos Campos, SP, Brazil

ARTICLE INFO

Article history:
Received 20 May 2015
Received in revised form
22 January 2016
Accepted 10 February 2016
Available online 12 February 2016

Keywords:
A. Sintering
Barium titanate
Layered ceramics
Dielectric
Ferroelectric and piezoelectric properties

ABSTRACT

The dielectric, pyroelectric and ferroelectric properties of bilayered $BaTiO_3/BaTi_{0.8}Zr_{0.2}O_3$ ceramics are described and correlated with their microstructure. Different sintering times are employed to change the microstructure and promote interdiffusion between the layers. The effects of constrained sintering on both compositions are analyzed and their properties are compared to that of single phase $BaTiO_3$ and $BaTi_{0.8}Zr_{0.2}O_3$ ceramics. The results show that, at sintering times until 2 h, the bilayer properties are predominantly affected by the presence of residual stresses. Only after 4 h sintering, the properties are predominantly affected by interdiffusion between the layers.

1. Introduction

Barium titanate ($BaTiO_3$) is a perovskite type (ABO_3) ferroelectric material [1] employed as main component in a variety of environmentall-friendly electronic devices such as memory storage systems, piezoelectric transducers, pyroelectric detectors and multi-layer ceramic capacitors [2–5]. However, in order to meet the technological requirements that these devices must satisfy, i.e. high dielectric constant, low dielectric loss and temperature stability of properties, $BaTiO_3$ must be modified [6], for example, by the development of layered ceramics. Using this approach, Ota et al. [7] produced $Ba_{1-x}Sr_xTiO_3$-based capacitors with a temperature-independent electrical permittivity. And Maurya et al. [8] showed that layered $BaTiO_3/0.975BaTiO_3–0.025Ba(Cu_{1/3}Nb_{2/3})O_3$ ceramics could be employed to better understand hysteresis dynamics to tailor their piezoelectric and ferroelectric properties.

Nevertheless, layered materials are generally affected by residual stresses due to thermal mismatch between the components [9]. Moreover, their microstructure and functional properties can also be affected by interdiffusion of atomic species while processing in high temperatures. Gopalan and Virkar [10,11] and Siao et al. [12] studied interdiffusion effects in $BaTiO_3$-based layered materials. According to their results, there is diffusion of all sublattices and the relations between the atomic diffusivities are $D_{Ti^{4+}} > D_{Zr^{4+}}$, $D_{Ti^{4+}} > D_{Ba^{2+}}$, $D_{O^{2-}} > D_{Ti^{4+}}$ and $D_{Ba^{2+}} > D_{Sr^{2+}}$. Therefore, Kirkendall effect [13] was observed in both cases.

The Kirkendall effect is the deviation, from it's initial position, of the contact plane between distinct materials after diffusion proceeded due to differences on atomic diffusion rates [14,15]. The effect was first observed on brass/copper samples and stated the importance of vacancies for the diffusional processes. Accordingly, and considering a bilayered sample for simplicity, a net vacancy flux is observed from the layer with slower (lower diffusion rates) atomic species towards the layer with faster (higher diffusion rates) atomic species. As consequences, the original contact plane moves together with the vacancies with a linearly dependence on the square root of time. Also, the vacancies concentration can reach saturation on the layer with faster atoms and vacancies precipitates as pores, known as Kirkendall porosity, while densification is expected on the slower atoms layer, in the case of ceramics. On the original α-brass-Cu diffusion couple [16], the initial interface moved towards the α-brass layer, together with Cu. Meanwhile Zn ($D_{Zn} > D_{Cu}$) diffused into the original Cu layer from the α-brass layer. Relative to the contact plane, the region in which Zn diffused was larger than the region in which Cu diffused and the relation between these regions is proportional to the ratio between the atomic diffusivities.

Gopalan and Virkar [10,11] identified the Kirkendall effect on ceramic diffusion pairs of the $BaTiO_3/BaZrO_3$ system. The effects of vacancy supersaturation was studied by introducing vacancies through acceptor (Sc) or donor (Ta) doping. According to their results, an increase on the number of Ba^{2+} vacancies through

* Corresponding author.
E-mail address: thimaral@ursa.ifsc.usp.br (T.M. Amaral).

http://dx.doi.org/10.1016/j.ceramint.2016.02.071
0272-8842/

acceptor dopant increased Kirkendall porosity on the Ti^{4+} rich layer. The system difussivity is limited by the slowest atom, Ba^{2+} in this case. Therefore an increase on Ba^{2+} vacancies increased it's diffusivity and stimulated Kirkendall effect. Moreover, they showed that Kirkendall effect and porosity are more prominent on coarse grained ceramics due to fewer vacancy sinks and, consequently, higher vacancy concentration and supersaturation.

Siao et al. [12] studied Kirkendall porosity in $BaTiO_3/SrTiO_3$ diffusion couples and established a parallel between their observations and the original α-brass-Cu diffusion couple. As $D_{Ba^{2+}}$ is higher than $D_{Sr^{2+}}$, Ba^{2+} diffused farther into the $SrTiO_3$, while vacancies precipitated as pores on the $BaTiO_3$ layer. Moreover, in the region in which Ba^{2+} diffused, core–shell structures with Ba^{2+}-rich shell were observed, meanwhile anomalous grains were observed growing from the interface towards the direction of the region in which Sr^{2+} had diffused. The anomalous grains were associated with an excess of Ti^{4+} (Ba^{2+} deficit) on the grain boundaries that grew at the expense of the smaller adjacent grains.

In a previous paper [17], we reported the functional properties of layered $BaTiO_3/BaTi_{1-x}Zr_xO_3$ ceramics. $BaTi_{1-x}Zr_xO_3$ is a solid solution in which Ti^{+4} ions are substituted by Zr^{+4}. Zr^{4+} is more chemically stable and a larger ion than Ti^{4+}, that leads to lower dielectric losses and a higher thermal stability of the electrical permittivity on the solid solution when compared to pure $BaTiO_3$ [10–13]. It was observed that the layers microstructures, after 2 h sintering, were very similar to those of single phase ceramics with correspondent compositions. Therefore, a correlation between the samples functional properties and residual stresses was reported without considering the effects associated with interdiffusion between the layers [17].

On this report we aim to observe effects that can be associated with interdiffusion, therefore, an increased Zr^{4+} concentration (20% of Ti^{4+} substitution in one of the layers) and increased sintering times were employed in order to maximize diffusion between the layers, while still retaining the ferroelectric/paraelectric phase transition above room temperature. It is observed that, after 2 h sintering, as reported previously, only effects related to residual stresses are observed. The effects due to interdiffusion become significant only on sintering times greater than 4 h. The effects are observed as modifications on the microstructure and on the evaluated functional properties, when compared with single phase $BaTiO_3$ ceramics and single phase $BaTi_{0.8}Zr_{0.2}O_3$ ceramics processed under the same conditions.

2. Experimental

$BaTiO_3$ and $BaTi_{0.8}Zr_{0.2}O_3$ powders were synthesized by the polymeric precursor route, as described elsewhere [18]. Barium acetate (99%, Alpha Aesar), Ti(IV)-isopropoxide (97%, Sigma Aldrich) and a Zr(IV)-propoxide solution (70% Sigma Aldrich) were separately mixed with water and citric acid (99.5%, Synth) in a molar relation of four citric acids to each metallic atom to produce aqueous metal citrates. After analysis of the metallic atom content, the citrates were mixed in the desired stoichiometric proportions; the pH was then controlled to 4 with NH_4OH and the temperature set to 80 °C. At this temperature, ethylene glycol (99.5%, Synth) was added in a mass proportion of 40:60 in relation to citric acid. The resultant transparent resin was treated at 400 °C for 4 h to eliminate organics, and a further treatment at 700 °C for 4 h was necessary to crystallize the desired $BaTiO_3$ and $BaTi_{0.8}Zr_{0.2}O_3$ powders. The final average particle sizes were 35 nm and 13 nm, respectively.

$BaTiO_3$, $BaTi_{0.8}Zr_{0.2}O_3$ and bilayered $BaTiO_3/BaTi_{0.8}Zr_{0.2}O_3$ ceramics were prepared by uniaxially pressing the powders under 30 MPa, one layer above the other in the case of the bilayers, and then isostatically pressing at 350 MPa to produce disc-shaped samples (6 mm diameter and 1 mm thick). The relative thermal expansion coefficient of single phase samples was measured (DIL 402 PC, NETZSCH, Selb, Germany) and the pellets were sintered at 1300 °C for 2 h, 4 h, 8 h, and 16 h. The heating rate was 5 °C/min while, at the end of the process, the oven was freely cooled down to room temperature.

The samples were mirror polished and the grains were developed at 1200 °C for 20 min with same heating and cooling conditions employed during sintering. The microstructure of the samples were analyzed by scanning electron microscopy (Inspect F-50, FEI, Hillsboro, USA) and the Zr^{4+} concentration profile across the interdiffusion region was obtained with line scan energy dispersive X-ray spectroscopy (EDX). The results from EDX analysis were used to confirm stoichiometry and to estimate the thicknesses of the interdiffusion region in the bilayered ceramics.

Gold electrodes were sputtered on parallel polished faces for dielectric, ferroelectric and piezoelectric measurements. The dielectric permittivity was measured in non-polarized samples from room temperature to 150 °C at a rate of 1 °C/min (FRA SI 1260 with dielectric interface 1296A, Solartron Analytical-Ametek, New York, USA). The simple series mixture rule

$$\frac{1}{\varepsilon} = \frac{\alpha}{\varepsilon_1} + \frac{1-\alpha}{\varepsilon_2}$$

was employed to calculate the expected electrical permittivity of the bilayered samples, with information about the volumetric fractions (α and $1-\alpha$) of the components and the temperature dependent dielectric permittivities (ε_1 and ε_2) of the single phase corresponding ceramics.

Ferroelectric hysteresis loops were measured in unpoled samples immersed in a silicone oil bath at 25 °C by applying a 10 Hz sinusoidal electric field with 3 kV/mm maximum amplitude. The pyroelectric coefficient was evaluated from the thermally stimulated depolarization current measured by a Sub-Femtoamperimeter (Model 6430, Keithley, Cleveland, USA) at a heating rate of 5 °C/min on samples poled in an oil bath with a 2.0 kV/mm electric field for 30 min at 25 °C.

3. Results and discussion

3.1. Single phase ceramics

Table 1 shows the relative density ($\rho_{\%}$, compared to $BaTiO_3$'s 6.02 g/cm^3) and the average grain size of single phase $BaTiO_3$ and $BaTi_{0.8}Zr_{0.2}O_3$ ceramics sintered for 2, 4, 8 and 16 h. As observed, the grain size and density of the $BaTiO_3$ ceramics are independent of sintering time and present values around 32 μm and 96%, respectively; on the other hand, in the $BaTi_{0.8}Zr_{0.2}O_3$ ceramics, grain sizes grow from 0.7 to 14 μm, while density increases from 97.5% to 99%, with sintering time changing from 2 to 16 h.

Fig. 1 presents the temperature dependence of the real permittivity for single phase $BaTiO_3$ and $BaTi_{0.8}Zr_{0.2}O_3$ ceramics sintered for 2, 4, 8 and 16 h, measured at 1 kHz. Table 2 contains the temperature of maximum permittivity (T_m), the Curie Weiss temperature (T_0) and the diffuseness degree of the phase transition (γ) obtained from adjusting the temperature-dependent electrical permittivity with the Curie–Weiss law and the modified Curie–Weiss law [19]. Regardless of sintering time, $BaTiO_3$ presents similar temperature dependence on the electrical permittivity, as well as similar T_m ($T_m \approx 121 \pm 1$ °C), T_0 ($T_0 \approx 110 \pm 1$ °C) and γ ($\gamma \approx 1.14 \pm 0.04$). The $BaTi_{0.8}Zr_{0.2}O_3$ samples present the same T_m ($T_m \approx 37 \pm 1$ °C), in spite of different grain sizes and regardless of sintering time. Also, T_0 for samples sintered for more

Table 1
Relative density and average grain size of single phase $BaTiO_3$ and $BaTi_{0.8}Zr_{0.2}O_3$ and bilayered $BaTiO_3/BaTi_{0.8}Zr_{0.2}O_3$ (BT/BZT20) ceramics for different sintering time.

Sintering time (h)	$BaTiO_3$		$BaTi_{0.8}Zr_{0.2}O_3$		$BaTiO_3/BaTi_{0.8}Zr_{0.2}O_3$ (BT/BZT20)		
	Relative density (%)	Average grain size (μm)	Relative density (%)	Average grain size (μm)	Relative density (%)	Average grain size (μm)	
						BT layer	BZT20 layer
2	95.7	31 ± 13	97.5	0.7 ± 0.4	97.1	35 ± 19	3 ± 2
4	96.2	34 ± 12	98.0	1.0 ± 05	97.0	30 ± 19	4 ± 2
8	95.8	30 ± 14	98.5	1.7 ± 0.9	96.5	32 ± 19	4 ± 2/* 174 ± 50
16	96.4	31 ± 16	99.0	17 ± 7	96.8	34 ± 16	104 ± 38

* At the interface.

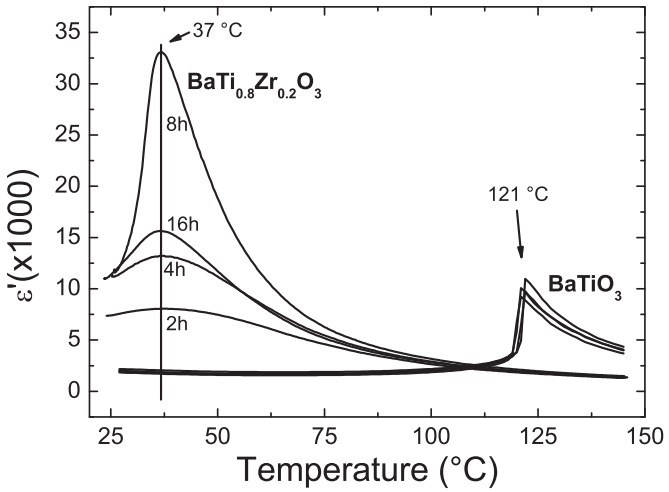

Fig. 1. Temperature-dependent electrical permittivity of the single phase ceramics for different sintering time, acquired at 1 kHz.

than 4 h is around the same value ($T_0 \approx 61 \pm 1$ °C). The grain size dependence is only observed on the permittivity's maximum amplitude and on the diffuseness degree of the phase transition (γ). A 2 h sintering process leads to $BaTi_{0.8}Zr_{0.2}O_3$ ceramics with diffuse phase transition and with the lowest electrical permittivity maximum amplitude, while 8 h sintering leads to the least diffuse phase transition and the highest electrical permittivity maximum.

The grain size dependence of $BaTi_{0.8}Zr_{0.2}O_3$ dielectric properties has been studied by many authors [20–25]. Their synthesis methodology and results (average grain size, T_m, T_0 and γ) are displayed in Table 3. Their data shows that, above 0.7 μm, T_m is, in most cases, independent of grain size, but insufficient data exists about T_0 to enable a proper evaluation of this parameter. Moreover, according to the literature, γ shows a grain size dependency, although there is conflicting information about the grain size effect. Thus, based on the literature and on the results presented on this paper, T_m is grain size independent on $BaTi_{0.8}Zr_{0.2}O_3$ ceramics.

Fig. 2 shows the heating dilatometry curve of single phase $BaTiO_3$ and $BaTi_{0.8}Zr_{0.2}O_3$ ceramics. The inset shows their cooling dilatometry curve from 1200 °C to room temperature, with the relative shrinkage values shifted to zero. It is observed that $BaTiO_3$ sintering begins 150 °C before $BaTi_{0.8}Zr_{0.2}O_3$, and that at the end of sintering there is a mismatch strain of about 0.09% between the samples. According to

Table 3
Literature data about grain size dependency of some $BaTi_{0.8}Zr_{0.2}O_3$ ceramics properties: the temperature of maximum permittivity (T_m), the Curie–Weiss temperature (T_0) and the diffuseness degree of the phase transition (γ).

Literature reference	Synthesis methodology	Average grain size (μm)	T_m (°C)	T_0 (°C)	γ
[20]	Commercial powder	0.7	~32	–	–
		1.23	~32		
		1.68	~32		
		33	~32		
		52	~32		
		68	~32		
		81	~32		
		96	~32		
[21]	Commercial powder	0.13	< 10	–	–
		0.2	< 10		
		1.9	37		
		3.7	37		
		21	37		
[23]	Solid state reaction	25	55	70	2.02
		45	50	68	1.93
		80	50	72	1.84
[22]	Sol gel	4	32	–	–
		8	32		
		25	32		
	Solid state reaction	15	42	–	–
[24]	Solid state reaction	25	18	40	1.60
		30	17	38	1.61
		47	14.5	38	1.66
		70	12	38	1.72
[25]	Sol gel	2	−4.4	−3.1	1.82
		15	23.5	26.46	1.78
		60	24.4	44.56	1.64

Table 2
Temperatures of maximum permittivity (T_m), Curie–Weiss temperature (T_0) and the phase transition diffuseness degree γ of single phase $BaTiO_3$ and $BaTi_{0.8}Zr_{0.2}O_3$ ceramics for different sintering times.

Sintering time (h)	$BaTiO_3$			$BaTi_{0.8}Zr_{0.2}O_3$		
	T_m (± 1 °C)	T_0 (± 1 °C)	γ (± 0.03)	T_m (± 1 °C)	T_0 (± 1 °C)	γ (± 0.03)
2	121	109	1.10	37	56	2.02
4	121	109	1.16	37	61	1.93
8	122	111	1.18	37	62	1.62
16	122	110	1.12	37	59	1.68

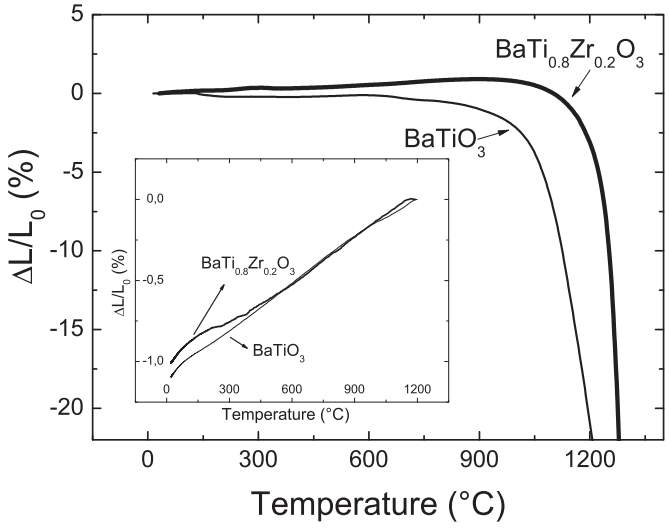

Fig. 2. Heating dilatometry results of homogeneous ceramics of $BaTiO_3$ and $BaTi_{0.8}Zr_{0.2}O_3$. The inset shows cooling dilatometry curves from 1200 °C with starting values shifted to zero.

these results, in a layered $BaTiO_3/BaTi_{0.8}Zr_{0.2}O_3$ ceramic, the Zr-rich layer is under compression during the initial stage of sintering. Nevertheless, as sintering proceeds, this stress due to differential sintering at the beginning of the process is expected to be damped by mass transport and grain movements at high temperatures [26,27]. At the end of the sintering process, after cooling the bilayered sample, the Zr-rich layer is once more under compression, while $BaTiO_3$ is strained due to $BaTiO_3$'s higher linear thermal expansion coefficient. Considering this case in a bilayer sample with volumetric fractions similar to the bilayer $BaTiO_3/BaTi_{0.8}Zr_{0.2}O_3$ sintered for 2 h, the mismatch strain would lead to a residual stress [9] of approximately 56 MPa on the $BaTiO_3$ layer and 29 MPa on the $BaTi_{0.8}Zr_{0.2}O_3$ layer (considering Young's Modulus of 67 GPa [28] and Poisson's ratio of 0.3 [29]). Other authors stated that, creep can damp stresses in $BaTiO_3$ above 1200 °C [26,27], therefore 1200 °C was selected as the cut-off temperature for calculating the residual stress.

3.2. Bilayered ceramics

Fig. 3 shows SEM micrographs of bilayered $BaTiO_3/BaTi_{0.8}Zr_{0.2}O_3$ ceramics sintered for 2, 4, 8 and 16 h. The average grain sizes and relative density of the composites are also summarized in Table 1. It is observed that the grain sizes of the $BaTiO_3$ layers on the composites are independent of sintering time and are around 32 μm. These grain sizes are the same presented by single phase $BaTiO_3$ ceramics; therefore $BaTiO_3$ microstructure is not affected by constrained sintering with $BaTi_{0.8}Zr_{0.2}O_3$. On the other hand, the $BaTi_{0.8}Zr_{0.2}O_3$ layers are affected by constrained sintering and by sintering time. The Zr-rich layer of the composites present average grain sizes of 3 and 4 μm when sintered for 2 and 4 h, respectively, and a dual grain size distribution with averages of

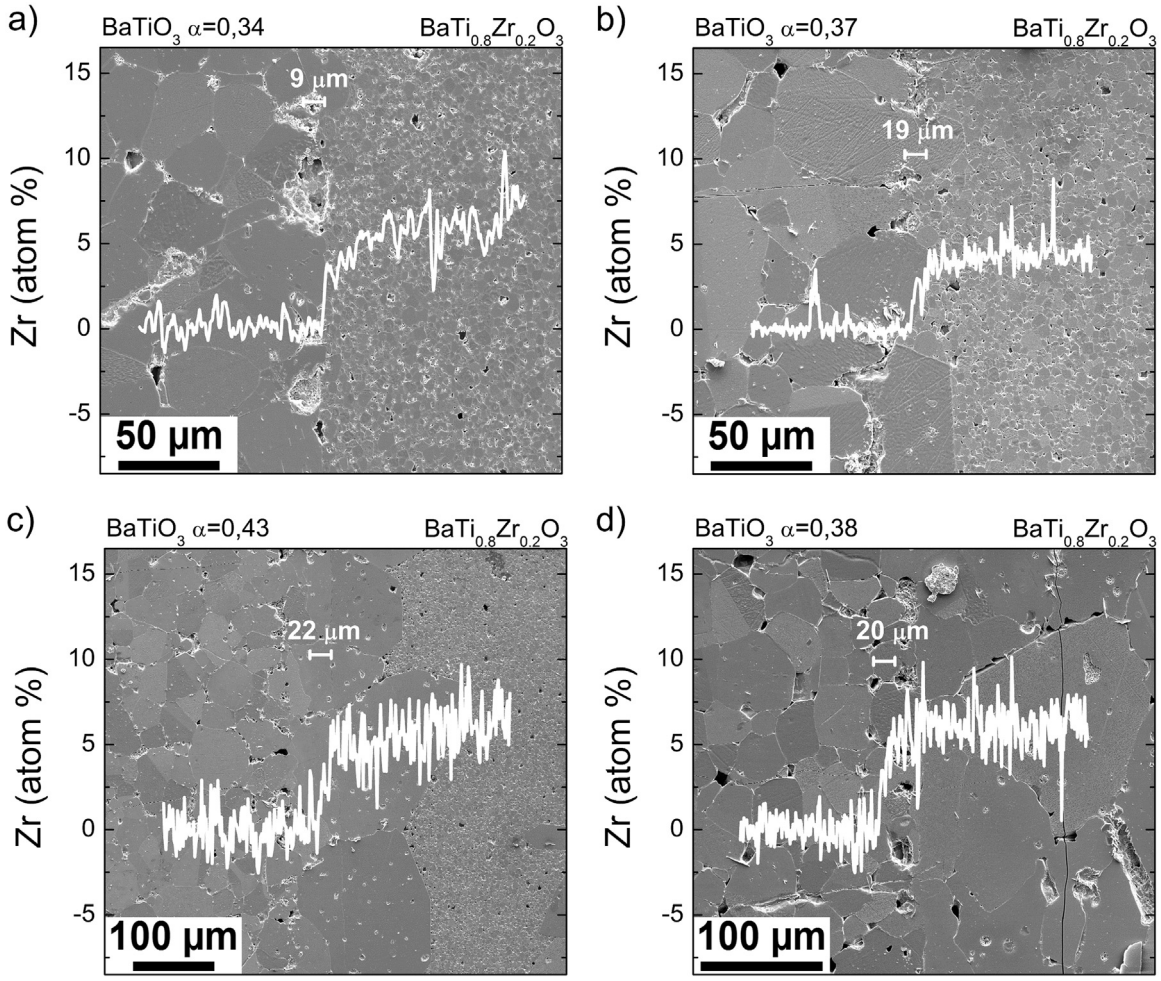

Fig. 3. SEM micrograph of bilayered $BaTiO_3/BaTi_{0.8}Zr_{0.2}O_3$ ceramics sintered for (a) 2 h, (b) 4 h, (c) 8 h and (d) 16 h. The composition, volumetric fraction (α) and interface thickness of each layer are displayed. Zirconium concentration profiles as a function of the longitudinal length are also presented in the micrographs.

4 and 174 μm, far from and close to the interdiffusion region, respectively, when sintered for 8 h (Fig. 2(c)), and an average grain size of 104 μm over the entire layer after 16 hours sintering (Fig. 2 (d)).

The micrographs of Fig. 3 also present the Zr concentration profile and the volumetric fraction of each layer. The Zr concentration profile for both layers far from the interdiffusion region agrees with the expected concentration independent of sintering time. Nevertheless, the interdiffusion region thickens from 9 μm in samples sintered for 2 h to a value of around 20 μm in samples sintered for 4, 8 and 16 h.

The differences in grain size between the single phase $BaTi_{0.8}Zr_{0.2}O_3$ ceramics and the layers can be accounted for the action of two different mechanisms that depend on the sintering stage. At early stages of sintering, the effect of compression stresses due to differential sintering (Fig. 2(a)) may change the contacts and increase mass transport between the $BaTi_{0.8}Zr_{0.2}O_3$ particles, as occurs in other sintering techniques such as hot pressing [30,31]. Nevertheless, this mechanism would readily be consumed by stress relaxation due to grain movements [9], therefore it cannot be responsible for the anomalous grain growth on samples sintered for higher times. After a long time at high sintering temperatures, the grain growth starting from the interdiffusion region between the layers is accounted for by the Kirkendall effect [14]. This was similarly described by Siao et al. [12] on $BaTiO_3/SrTiO_3$ diffusion couples. As Ba^{2+} diffused towards the $SrTiO_3$ faster than Sr^{2+} diffused toward the $BaTiO_3$ layer, grains with Ti^{4+} rich boundaries at the $BaTiO_3$ layer grew at the expense of smaller adjacent grains. In the case of $BaTiO_3/BaTi_{0.8}Zr_{0.2}O_3$ diffusion couple, the Ti^{4+}-rich grain boundaries are expected to be on the Zr^{4+}-rich layer due to the higher diffusivity of the Ti^{4+} compared with that of Zr^{4+} [11]. Therefore, the anomalous grain growth is observed, as expected, at the $BaTi_{0.8}Zr_{0.2}O_3$ layer.

Fig. 4 presents the temperature dependence of the real permittivity of the bilayered $BaTiO_3/BaTi_{0.8}Zr_{0.2}O_3$ ceramics sintered for different times, together with calculated expected values by the simple mixture rule. Fig. 4(a) shows the results for the bilayer sintered for 2 h. The peaks correspond to the phase transition of the $BaTi_{0.8}Zr_{0.2}O_3$ and of the $BaTiO_3$ at 37 °C and 128 °C, respectively. It is observed that an agreement exists between the calculations and the experimental amplitudes, although there is a shift on the temperature of the experimental $BaTiO_3$ transition peak toward a higher temperature. This $BaTiO_3$ layer presents the same microstructure as single phase $BaTiO_3$ samples. Therefore, the temperature shift cannot be associated with any grain size effect. The peak is shifted in 7 ± 2 °C; a much higher value than the differences among the homogeneous samples and this shift corresponds to the effect of a two-dimensional stress of 140 ± 20 MPa, according to Jaffe (for ceramics) [32], or 41 ± 7 MPa according to Forsbergh (for single crystals) [33], the same order of magnitude as calculated by the thermal mismatch (56 MPa). The permittivity peak corresponding to $BaTi_{0.8}Zr_{0.2}O_3$ layer does not present a shift when compared to homogeneous samples. However, this layer is subjected to a lower stress and, to our knowledge, there are no reports concerning two-dimensional stress effects for this composition.

The subsequent Fig. 4(b)–(d) shows results for the bilayers sintered for 4, 8 and 16 h, respectively. At these increased sintering times, the shift in temperature of the experimental $BaTiO_3$'s transition is reduced to a value of 3 ± 2 °C, which means that the two-dimensional stresses on these samples are lower than those on the samples sintered for 2 h. This damping in the stresses is attributed to the increase of the interdiffusion region (Fig. 3) and, possibly to cracks, as observed in Fig. 4(d). A thicker interdiffusion region has a smoother compositional gradient, which reduces the thermal mismatch as in a functionally graded material [34]. On the

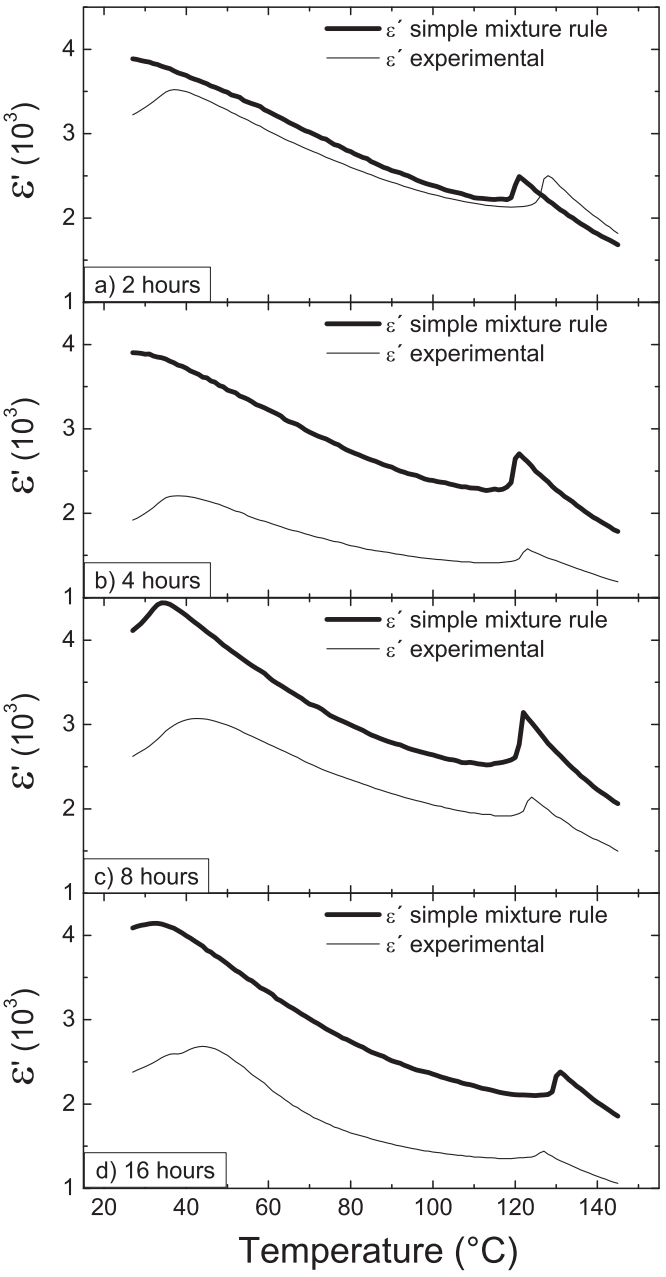

Fig. 4. Experimental and predicted temperature dependent real permittivity of bilayered $BaTiO_3/BaTi_{0.8}Zr_{0.2}O_3$ ceramics sintered for **a)** 2 hours, **b)** 4 hours, **c) 8** hours and **d)** 16 hours.

contrary, the temperature corresponding to the $BaTi_{0.8}Zr_{0.2}O_3$ permittivity peaks on sintering times of 8 and 16 h (42 °C and 45 °C, respectively) is much higher than that of the single phase $BaTi_{0.8}Zr_{0.2}O_3$ ceramics (37 °C). Since T_m is independent of grain size and residual stresses are discarded for these layers, these shifts are attributed to the compositional change on a fraction of the $BaTi_{0.8}Zr_{0.2}O_3$ layer, as consequence of the Kirkendall effect, also observed by Siao et al. [12]. During sintering, Ti^{4+} (and Zr^{4+}) diffuses towards the Zr^{4+}-(or the Ti^{4+}-) rich layer, thereby reducing the effective Zr^{4+} (or Ti^{4+}) amount on the region close to the interface. The result is a change on the composition of the $BaTi_{0.8}Zr_{0.2}O_3$ (or $BaTiO_3$) layer to $BaTi_{0.8+\delta}Zr_{0.2-\delta}O_3$ (or $BaTi_{1-\delta}Zr_{\delta}O_3$). Consequently, this mechanism produces an increase in the local Curie-temperature at the $BaTi_{0.8}Zr_{0.2}O_3$ layer as well as a decrease at the Curie temperature at the $BaTiO_3$ layer around the interface. Nevertheless, as Ti^{4+} has a higher diffusion rate than

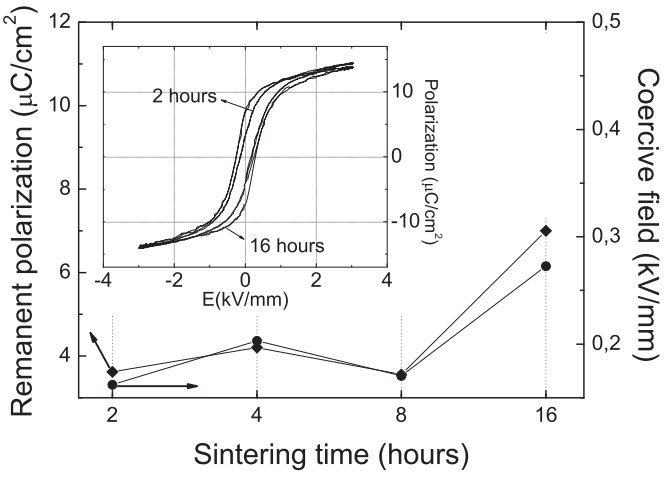

Fig. 5. Remanent polarization (P_r) and coercitive fields (F_c) of bilayered $BaTiO_3/BaTi_{0.8}Zr_{0.2}O_3$ ceramics sintered for 2, 4, 8 and 16 h. The inset shows hysteresis loops of bilayered samples sintered for 2 and 16 h.

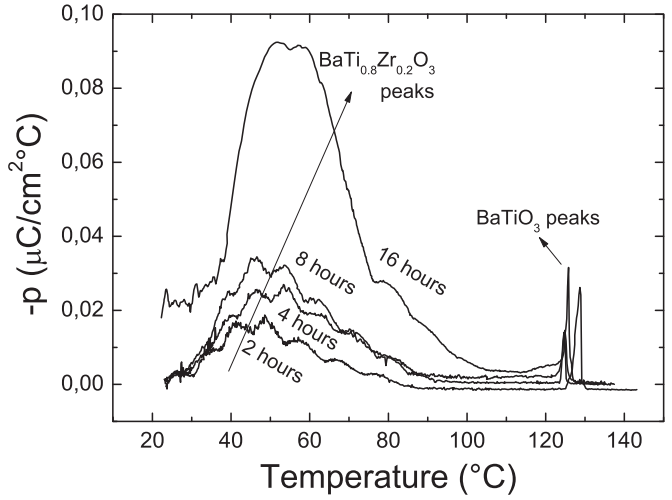

Fig. 6. Temperature dependent pyroelectric coefficient of bilayered $BaTiO_3/BaTi_{0.8}Zr_{0.2}O_3$ ceramics sintered for 2, 4, 8 and 16 h.

Zr^{4+}, farther the Ti^{4+} ions can diffuse toward the $BaTi_{0.8}Zr_{0.2}O_3$ layer than the Zr^{4+} diffuses toward the $BaTiO_3$ layer, therefore the affected region on the $BaTi_{0.8}Zr_{0.2}O_3$ layer is much larger than the affected region at the $BaTiO_3$ layer. Consequently, interdiffusion effects are expected to be observed on the properties associated with the $BaTi_{0.8}Zr_{0.2}O_3$ and to become more significant with increasing sintering time. Moreover, it is also observed that the electrical permittivity of bilayered samples presents lower amplitudes than calculated by the simple mixture rule. As regards the consequences of the Kirkendall effect, Kirkendall porosity is expected on the region with the fastest ions (here, the $BaTiO_3$ layer) as observed by the other authors [11,12]. Nevertheless, as Siao et al. observed, the Kirkendall pores could be of the order of tenths of nanometers, therefore, not observed in our case. In this sense, this region with Kirkendall porosity and possibly also cracks contribute with a layer of lower electrical permittivity that was not considered during calculations but were responsible for the reduced total permittivity of the composite.

Fig. 5 shows remanent polarization (P_r) and coercive fields (F_c) for bilayers sintered for 2, 4, 8 and 16 h, while the inset shows the hysteresis loops of the bilayers sintered for 2 and 16 h at room temperature. Comparing the samples sintered for 2 and 16 h, it is observed that the P_r and the F_c increase from 3.6 ± 0.3 to 7.0 ± 0.2 μC/cm^2 and from 0.16 ± 0.02 to 0.27 ± 0.04 kV/mm, respectively. This higher polarization of the samples sintered for 16 hours is expected due to the presence of a larger region with $BaTi_{0.8+\delta}Ti_{0.2-\delta}O_3$ composition than the samples sintered for 2 h.

Fig. 6 shows the temperature-dependent pyroelectric coefficient of the bilayers sintered for 2, 4, 8 and 16 h. Two main contributions are observed in each curve: i) a sharp peak around 125 °C associated with the $BaTiO_3$ phase transition, and ii) a broad peak around 30 °C associated with the $BaTi_{0.8}Zr_{0.2}O_3$ phase transition. Among the peaks corresponding to $BaTiO_3$, a shift towards higher temperatures is observed only on samples sintered for 2 hours, as also visualized in Fig. 4(a), due to the presence of residual stresses. Nevertheless, there is a shift of the maximum temperature toward higher values and an increase on both the amplitude and the broadness of the peaks corresponding to the $BaTi_{0.8}Zr_{0.2}O_3$ layer with increase on sintering time. These modifications are in agreement with compositional changes derived from Kirkendall effect.

Another explanation for the differences in the ferroelectric and pyroelectric properties of the bilayered samples sintered for 2 and 16 h could be related to an effect of preferential crystallographic orientation of the $BaTi_{0.8}Zr_{0.2}O_3$ grains, with the polar axis pointing in an orthogonal direction to the electrode plane [35]. Nevertheless, X-ray diffraction pattern of the $BaTi_{0.8}Zr_{0.2}O_3$ layer yields no differences between the samples, regardless of the grain sizes.

4. Conclusions

Dielectric, pyroelectric and ferroelectric properties of bilayered $BaTiO_3/BaTi_{0.8}Zr_{0.2}O_3$ ceramics sintered for different times are described and correlated with their microstructure. It is concluded that two different mechanisms are responsible for the observed differences on the bialyers properties compared to single phase ceramics. On the samples sintered for short times, the temperature shift of $BaTiO_3$ Curie-temperature, the narrow interdiffusion region and the features presented by the microstructure suggest that residual stresses after cooling constitute the main factor affecting the properties of the samples. On the other hand, on bilayered samples sintered for times longer than 4 h, the effects due to interdiffusion between the layers are more significant than residual stresses. In this sense, the Kirkendall effect is identified as being responsible for the anomalous grain growth, the increased pyroelectric coefficient and the temperature shift of maximum permittivity on the $BaTi_{0.8}Zr_{0.2}O_3$ layer, as well as the overall decrease in the composite electrical permittivity when compared to calculations with the simple mixture rule.

References

[1] G.H. Haertling, Ferroelectric ceramics: history and technology, J. Am. Ceram. Soc. 82 (1999) 797–818, http://dx.doi.org/10.1111/j.1151-2916.1999.tb01840.x.
[2] T.R. Shrout, S.J. Zhang, Lead-free piezoelectric ceramics: alternatives for PZT? J. Electroceram. 19 (2007) 111–124, http://dx.doi.org/10.1007/s10832-007-9047-0.
[3] T. Karaki, K. Yan, T. Miyamoto, M. Adachi, Lead-free piezoelectric ceramics with large dielectric and piezoelectric constants manufactured from $BaTiO_3$ nanopowder, Jpn. J. Appl. Phys. 46 (2007) L97–L98, http://dx.doi.org/10.1143/JJAP.46.L97.
[4] H. Kishi, Y. Mizuno, H. Chazono, Base-metal electrode-multilayer ceramic capacitors: past, present and future perspectives, Jpn. J. Appl. Phys. 42 (2003) 1–15, http://dx.doi.org/10.1143/JJAP.42.1.
[5] A.C. Randall, Scientific and engineering issues of the state-of-the-art and future multilayer capacitors, J. Ceram. Soc. Jpn. 109 (2001) 2–6.
[6] H.-W. Lee, M.S.H. Chu, H.-Y. Lu, Phase mixture and reliability of $BaTiO_3$-based X7R multilayer ceramic capacitors: X-ray diffractometry and Raman spectroscopy, J. Am. Ceram. Soc. 94 (2011) 1556–1562, http://dx.doi.org/10.1111/j.1551-2916.2010.04248.x.
[7] T. Ota, Y. Abe, T. Hirashita, H. Myazaki, Y. Hikichi, H. Suzuki, Flat profile of permittivity vs temperature for graded $Ba_{1-x}Sr_xTiO_3$ ceramics, J. Ceram. Soc.

Jpn. 109 (2001) 174–176.
[8] D. Maurya, N. Wongdamnern, R. Yimnirun, S. Priya, Dielectric and ferroelectric response of compositionally graded bilayer and trilayer composites of $BaTiO_3$ and $0.975BaTiO_3$–$0.025Ba(Cu_{1/3}Nb_{2/3})O_3$, J. Appl. Phys. 108 (2010) 124111, http://dx.doi.org/10.1063/1.3514125.
[9] L. Sestakova, R. Bermejo, Z. Chlup, R. Danzer, Strategies for fracture toughness, strength and reliability optimisation of ceramic-ceramic laminates, Int. J. Mater. Res. 102 (2011) 613–626, http://dx.doi.org/10.3139/146.110523.
[10] S. Gopalan, A.V. Virkar, Interdiffusion and Kirkendall effect in doped barium titanate-strontium titanate diffusion couples, J. Am. Ceram. Soc. 78 (1995) 993–998, http://dx.doi.org/10.1111/j.1151-2916.1995.tb08427.x.
[11] S. Gopalan, A.V. Virkar, Interdiffusion and Kirkendall effect in doped $BaTiO_3$ –$BaZrO_3$ perovskites: effect of vacancy supersaturation, J. Am. Ceram. Soc. 82 (1999) 2887–2899, http://dx.doi.org/10.1111/j.1151-2916.1999.tb02173.x.
[12] C.-Y. Siao, H.-W. Lee, H.-Y. Lu, Kirkendall porosity in barium titanate–strontium titanate diffusion couple, Ceram. Int. 35 (2009) 2951–2958, http://dx.doi.org/10.1016/j.ceramint.2009.04.009.
[13] F. Seitz, On the porosity observed in the Kirkendall effect, Acta Metall. 1 (1953) 355–369, http://dx.doi.org/10.1016/0001-6160(53)90112-6.
[14] A. Paul, M.J. van Dal, A. Kodentsov, F.J. van Loo, The Kirkendall effect in multiphase diffusion, Acta Mater. 52 (2004) 623–630, http://dx.doi.org/10.1016/j.actamat.2003.10.007.
[15] H. Nakajima, The discovery and acceptance of the Kirkendall effect: the result of a short research career, JOM 49 (1997) 15–19, http://dx.doi.org/10.1007/BF02914706.
[16] A.D. Smigelskas, E.O. Kirkendall, Zinc diffusion in alpha brass, Trans. AIME 171 (1947) 130–142.
[17] T.M. Amaral, E. Antonelli, D.A. Ochoa, J.E. García, A.C. Hernandes, Microstructural features and functional properties of bilayered $BaTiO_3/BaTi_{1-x}Zr_xO_3$ Ceramics, J. Am. Ceram. Soc. 98 (2015) 1169–1174, http://dx.doi.org/10.1111/jace.13417.
[18] M.I.B. Bernardi, E. Antonelli, A.B. Louren, C.A.C. Feitosa, L.J.Q. Maia, A. C. Hernandes, $BaTi_{1-x}Zr_xO_3$ nanopowders prepared by the modified Pechini method, J. Therm. Anal. Calorim. 87 (2007) 725–730.
[19] K. Uchino, S. Nomura, Critical exponents of the dielectric constants in diffused-phase-transition crystals, Ferroelectrics 44 (1982) 55–61, http://dx.doi.org/10.1080/00150198208260644.
[20] Y. Hirata, T. Kawazoe, Wet forming, sintering behavior, and dielectric properties of $BaTi_{0.8}Zr_{0.2}O_3$, J. Mater. Res. 11 (2011) 3071–3076, http://dx.doi.org/10.1557/JMR.1996.0390.
[21] T. Hoshina, T. Furuta, T. Yamazaki, H. Takeda, T. Tsurumi, Grain size effect on dielectric properties of Ba (Zr,Ti)O_3 ceramics, Jpn. J. Appl. Phys. 51 (2012) 09LC04–1, http://dx.doi.org/10.1143/JJAP.51.09LC04.
[22] S. Kazaoui, J. Ravez, Dielectric relaxation in $Ba(Ti_{0.8}Zr_{0.2})O_3$ ceramics prepared from sol–gel and solid state reaction powders, J. Mater. Sci. 28 (1993) 1211–1219, http://dx.doi.org/10.1007/BF01191955.
[23] C. Fu, F. Pan, W. Cai, X. Deng, Relaxor behavior of $BaZr_{0.2}Ti_{0.8}O_3$ ceramics with different grains, Integr. Ferroelectr. 104 (2008) 1–7, http://dx.doi.org/10.1080/10584580802554844.
[24] Z. Sun, L. Li, H. Zheng, S. Yu, D. Xu, Effects of sintering temperature on the microstructure and dielectric properties of $BaZr_{0.2}Ti_{0.8}O_3$ ceramics, Ceram. Int. 41 (2015) 12158–12163, http://dx.doi.org/10.1016/j.ceramint.2015.06.035.
[25] X.G. Tang, J. Wang, X.X. Wang, H.L.W. Chan, Effects of grain size on the dielectric properties and tunabilities of sol–gel derived $Ba(Zr_{0.2}Ti_{0.8})O_3$ ceramics, Solid State Commun. 131 (2004) 163–168, http://dx.doi.org/10.1016/j.ssc.2004.05.016.
[26] E.T. Park, P. Nash, J. Wolfenstine, K.C. Goretta, J.L. Routbort, High-temperature creep of polycrystalline $BaTiO_3$, J. Mater. Res. 14 (1999) 523–528 (accessed 01.10.14) http://journals.cambridge.org/abstract_S0884291400047762.
[27] C. Carry, A. Mocellin, Superplastic creep of fine grained $BaTiO_3$ in a reducing environment, J. Am. Ceram. Soc. 69 (1986) 215–216 (accessed 01.10.14) http://onlinelibrary.wiley.com/doi/10.1111/j.1151-2916.1986.tb07483.x/abstract.
[28] T. Sakakibara, H. Izu, T. Kura, W. Shinohara, H. Iwata, S. Kiyama, et al., No Title, Proc. of the IEEE 5th Int. Symp. Micro Mach. Hum. Sci., 1994. p. 75.
[29] A.C. Dent, C.R. Bowen, R. Stevens, M.G. Cain, M. Stewart, Effective elastic properties for unpoled barium titanate, J. Eur. Ceram. Soc. 27 (2007) 3739–3743, http://dx.doi.org/10.1016/j.jeurceramsoc.2007.02.031.
[30] R.L. Coble, Diffusion models for hot pressing with surface energy and pressure effects as driving forces, J. Appl. Phys. 41 (1970) 4798, http://dx.doi.org/10.1063/1.1658543.
[31] M. Demartin, C. Hérard, C. Carry, J. Lemaître, Dedensification and anomalous grain growth during sintering of undoped barium titanate, J. Am. Ceram. Soc. 80 (2005) 1079–1084, http://dx.doi.org/10.1111/j.1151-2916.1997.tb02949.x.
[32] H. Jaffe, D. Berlincourt, J. McKee, Effect of pressure on the Curie temperature of polycrystalline ceramic barium titanate, Phys. Rev. 105 (1957) 57–58, http://dx.doi.org/10.1103/PhysRev.105.57.
[33] P. Forsbergh, Effect of a two-dimensional pressure on the Curie point of barium titanate, Phys. Rev. 93 (1954) 686–692, http://dx.doi.org/10.1103/PhysRev.93.686.
[34] S. Schmauder, U. Weber, Modelling of functionally graded materials by numerical homogenization, Arch. Appl. Mech. 71 (2001) 182–192, http://dx.doi.org/10.1007/s004190000124.
[35] B. Jaffe, R.W. Cook, H.L. Jaffe, Piezoelectric Ceramics, Academic Press, London, 1971.